ELSEVIER

Polymer 42 (2001) 4635–4646

polymer

www.elsevier.nl/locate/polymer

Dual crystalline texture in HDPE blown films and its implication on mechanical properties

J. Lu[a], H.-J. Sue[a,*], T.P. Rieker[b]

[a]Department of Mechanical Engineering, Polymer Technology Center, Texas A & M University, College Station, TX 77843-3123, USA
[b]Department of Chemical and Nuclear Engineering, Center for Microengineered Materials, University of New Mexico, Albuquerque, NM 87131, USA

Received 7 April 2000; received in revised form 7 September 2000; accepted 21 September 2000

Abstract

The morphological features of a series of high-density polyethylene (HDPE) blown films were studied using transmission electron microscopy, small-angle X-ray scattering and infrared dichroism. An orthogonally-oriented, dual crystalline texture was found in these HDPE films. This structure appears to consist of two superimposed row-oriented textures. In one row-oriented texture, the lamellae are stacked along the machine direction; while in the other, the lamellae are stacked along the transverse direction. The lamellar populations in the two textures are greatly affected by the neck height of the film blowing process. The mechanical properties of the films correlate well with the observed dual crystalline texture.

Keywords: Polyethylene; HDPE; Blown film

1. Introduction

Polyethylene (PE) blown film is one of the most important polymeric products consumed today. PE film manufacturers have been aggressive in improving film properties and reducing production cost so that they can be more competitive in the global market. Information concerning blown film structure and structure–property relationship is important to PE film manufacturers. The study of film structure can provide the knowledge about the structural formation process during film blowing and, in turn, the effect of processing conditions on film properties. Moreover, blown film is a good candidate for studying crystallization processes of polymers under stress. Therefore, investigation of the structure of PE blown films has been the focus of significant research efforts.

The study of the structure of extruded PE films started in the 1950s. Holmes et al. [1] studied the structures of melt-extruded low-density polyethylene (LDPE) blown films using a Statton X-ray camera, and concluded that the *a*-axis of the crystal unit cell lies along the extrusion direction. This finding was confirmed by Aggarwal et al. [2], who concluded that the crystallographic *a*-axis in PE blown film is oriented along the machine direction (MD), while the *b*- and *c*-axes are randomly distributed in the plane perpendicular to the *a*-axis. In 1954, Keller [3,4] proposed that the crystal *b*-axis in PE blown films has a preferred orientation perpendicular to the MD while the *a*- and *c*-axes are randomly distributed with cylindrical symmetry. He also introduced the concept of row orientation in which the crystalline lamellar overgrowth occurs epitaxially from the *c*-axis oriented fibrils with radial growth in the *b*-direction and the *a*- and *c*-axes rotating about that growth direction. Using the method of pole figures for high-density polyethylene (HDPE) extruded films, Lindenmeyer and Lustig [5] found support for the row structure.

In 1967 Keller and Machin [6] further modified the model of 'row nuclei' based on the level of stress for both LDPE and HDPE extruded films. According to the modified model, two major crystallization processes take place depending upon the magnitude of the stress in the melt, namely 'low-stress' and 'high-stress' crystallizations. Under low-stress conditions, the lamellae grow radially outward in the form of twisted ribbons, with the crystallographic *b*-axis parallel to their growth axis. As a result of this lamellar growth process, the *a*-axis of the crystal unit cell is oriented preferentially along the MD of the blown film. This texture is referred to as the Keller/Machin I morphology or *a*-texture. Under high-stress conditions, the radially grown lamellae extend directly outward without

* Corresponding author. Tel.: +1-979-845-5024; fax: +1-979-862-3989.
E-mail address: hjsu@acs.tamu.edu (H.-J. Sue).

0032-3861/01/$ - see front matter
PII: S0032-3861(00)00719-9

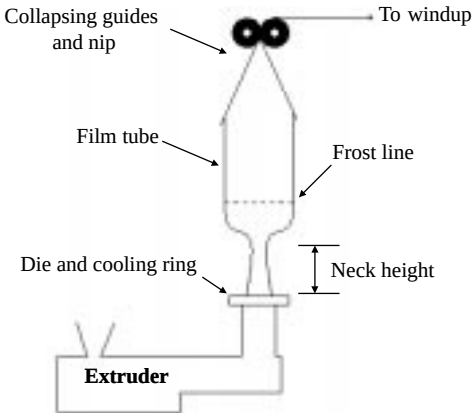

Fig. 1. Schematic of the film blowing process.

twisting. The folded chains (*c*-axis) within the lamellae remain parallel to the extended microfibers, resulting in the *c*-axis oriented preferentially along the MD. This is referred to as the Keller/Machin II morphology or *c*-texture. Intermediate stresses will lead to an incomplete twisting of the ribbons. This row nuclei model has been commonly used in the literature to describe the structures of PE blown films. The Keller/Machin I morphology is the most commonly observed morphology in PE blown films [5,7–13]. The Keller/Machin II morphology has been observed only in HDPE blown films [13–15].

In the 1970s, Maddams and Preedy published a series of papers based on an extensive texture investigation of very different HDPE blown films [12–14]. The orientation maxima of the crystallographic *a*-, *b*-, and *c*-axes were related to the stress levels at crystallization. Notably, they found an additional orientation maximum of the *b*-axis in the normal direction (ND) connected with the transcrystalline portion of the material.

Since the crystalline textures of tubular blown films are formed by different parallel crystallization and orientation processes, it is possible that a multiple-texture crystalline phase is formed in blown films. Choi et al. [16] used wide-angle X-ray scattering (WAXS), small-angle X-ray scattering (SAXS) and birefringence to characterize films fabricated under conditions ranging from uniaxial to biaxial extension, with concurrent measurements of the MD and TD stresses at the frost line. They proposed morphologies that consist of local lamellar stacks. The distribution of stack orientations is determined by the MD/TD stress balance at crystallization. Kwack and Han [17] found that the biaxial stress ratio is the determining factor in the distribution of fibrillous nuclei and crystalline texture, as well as film anisotropy. Later, Dormier et al. [18] presented their finding of a dual crystalline texture in high molecular weight HDPE blown films. However, not much work has been done so far to address in detail the effect of the local lamellar stacks and their orientation distribution on mechanical properties of blown films.

Recently, Wilkes et al. investigated the molecular orientation and processing–structure–property (P–S–P) relationships in uniaxially melt-extruded HDPE films possessing a well-defined, stacked lamellar morphology [15,19]. Their work greatly contributed to the understanding of the micro-mechanical deformation mechanisms and orientation-dependent mechanical properties of PE blown films. However, most commercial PE films are made by blowing processes with biaxial extension. Films with biaxial orientation need to be considered in greater detail.

As part of a continuing effort toward a better understanding of P–S–P relationships in PE blown films, a series of HDPE blown films were studied. This paper will present our experimental findings regarding the morphology of HDPE blown films and their correlation with mechanical properties. The effect of processing conditions on morphological characteristics will be discussed as well.

2. Experimental

2.1. Materials

Five HDPE blown films were provided by the Polyolefins Film Consortium at Texas A & M University. They were blown from three different HDPE resins. Films A-1, A-2 and

Table 1
Resin properties and processing parameters for the HDPE blown films studied

Films	A-1	A-2	A-3	B-1	C-1
Density (g/cm^3)	0.949	0.949	0.949	0.949	0.949
Melt index (g/10 min)	0.05	0.05	0.05	0.06	0.02
Thickness (μm)	12	12	12	12	12
M_n	7500	7500	7500	7500	6300
M_w	148,000	148,000	148,000	158,000	175,000
Die diameter (mm)	160	160	160	160	160
Die gap (mm)	1.5	1.5	1.5	1.5	1.5
Melt temperature (°C)	193	193	193	189	196
Draw up ratio	31	31	31	31	31
Blow up ratio	4/1	4/1	4/1	4/1	4/1
Neck height (DD)	6	8	10	8	8

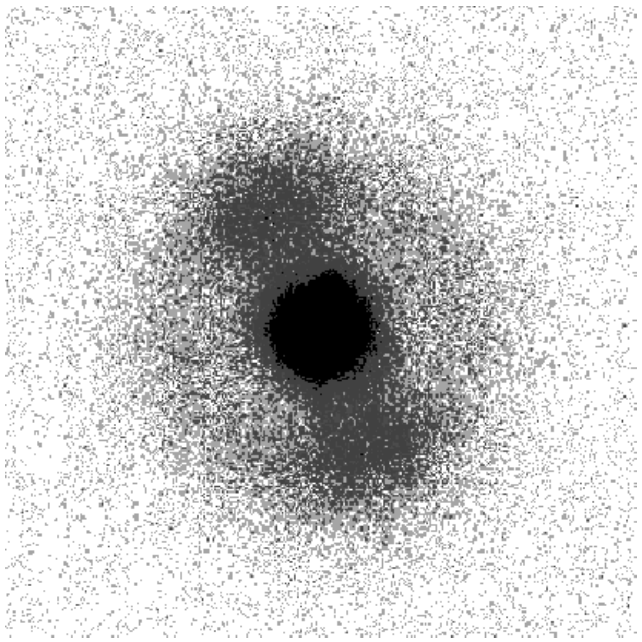

Fig. 2. Two-dimensional SAXS image taken in long geometry for film A-1. The film is oriented perpendicular to the incident X-ray beam. Therefore, the image shows preferred orientation in the MD–TD plane of the sample.

A-3 were blown from resin A with the same processing parameters, except for variation in neck heights (Fig. 1). The neck heights for A-1, A-2 and A-3 are 6, 8 and 10 die diameters (DD), respectively. Films B-1 and C-1 were produced from resins B and C, respectively. The neck height used for films B-1 and C-1 was the same as that used for film A-2, i.e. 8 DD. For convenience, films A-1, A-2 and A-3 are called Series I and films A-2, B-1 and C-1 are called Series II. Information about the resin properties and the blown film processing conditions is given in Table 1.

2.2. Infrared dichroism

A Nicolet Avatar 360 Fourier Transform Infrared (FTIR) Spectrometer equipped with a polarizer was used to determine IR dichroism of the films. The absorption bands at 730 and 719 cm^{-1} were employed to evaluate the orientations of the crystal *a*-axis and *b*-axis, respectively. The spectral separation procedure described by Kissin [20] was used to obtain the real absorbance from the measured absorbance of the bands. Dichroic ratio (D) was taken as the ratio of the absorbance measured with radiation polarized in the MD to that measured with radiation polarized in the TD. The method developed by Read and Stein [21] was used to calculate the orientation functions of crystal axes f_a, f_b and f_c.

2.3. Transmission electron microscopy

Samples for the transmission electron microscopy (TEM) study were embedded in an epoxy and cured overnight at room temperature. The blocks were trimmed, faced-off, and then stained with RuO_4 vapor ($RuCl_3$ + aqueous sodium hypochlorite). Ultra-thin sections, ranging from 60 to 80 nm, were obtained using a Reichert–Jung Ultracut E microtome with a diamond knife. The thin sections were placed on 100-mesh Formvar-coated copper grids and examined using a Zeiss-10C TEM operating at an accelerating voltage of 100 kV.

2.4. Small angle X-ray scattering

The SAXS measurements were carried out at the University of New Mexico/Sandia National Laboratories SAXS laboratory [22]. Samples and backgrounds were run on the 5-m pinhole instrument in both long and short geometry configurations with sample to detector distances of 248 and 31 cm, respectively. When combined, the data sets span a q-range of $0.003 < q < 0.7$ $Å^{-1}$, where $q = 4\pi/\lambda \sin(2\theta/2)$. Here, λ is the wavelength of the radiation, and θ is the radial scattering angle. SAXS samples were prepared by carefully folding the blown films into eight layers, and maintaining the MD of each layer parallel to every other. This produced samples with 0.12 mm in thickness. The samples were mounted on a sample changer such that the incident X-ray beam was normal to the plane of the films and that the MD was oriented in the beam with the same direction for all samples.

2.5. Tensile tests

The engineering stress–strain curves and Young's moduli of the blown films were obtained using a screw-driven mechanical testing machine (Instron, Model 1125) at ambient conditions. To obtain engineering stress–strain curves, specimens with dimensions of 50 mm × 12.7 mm ($2'' \times 0.5''$) were stretched at a cross-head speed of 50 mm/min ($2''$/min) either to breaking or to the limit of the instrument. The Young's moduli were determined by straining specimens with dimensions of 254 mm × 12.7 mm ($10'' \times 0.5''$) at a cross-head speed of 25 mm/min ($1''$/min), following the ASTM D882-95a method.

3. Results and discussion

3.1. Morphological investigation

Fig. 2 shows the as-collected two-dimensional (2D) SAXS pattern of film A-1, taken in long geometry. The presence of a preferred orientation of the lamellae within this sample is immediately evident from the anisotropic scattering pattern. In such a 2D image, the scattering angle 2θ is zero at the center and increases with radius. The azimuthal angle, X locates the scattering features around the detector. X is set to zero at the 6 o'clock position

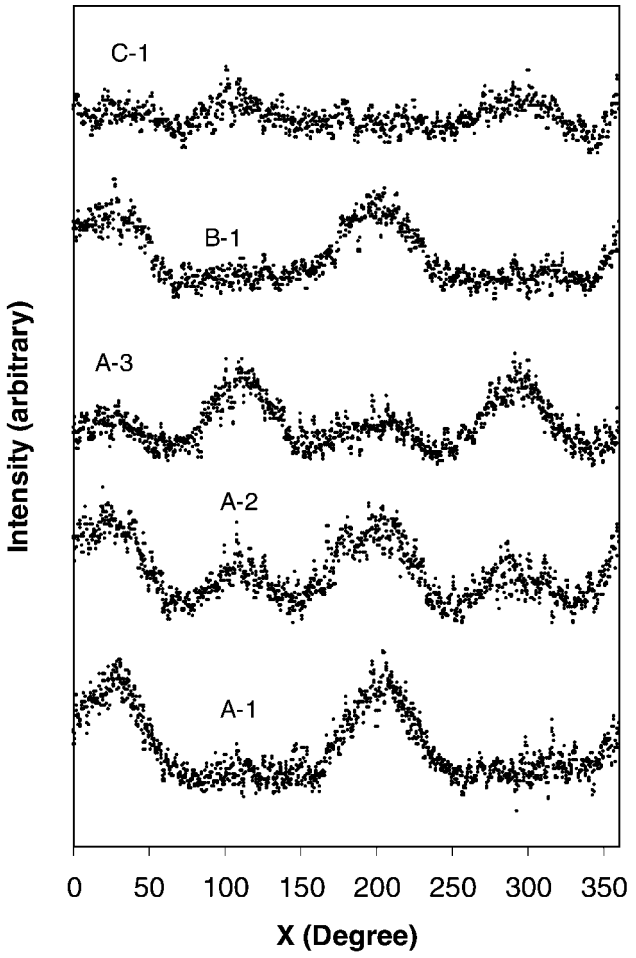

Fig. 3. SAXS intensity vs. X plots of the five HDPE blown films. The plots are generated by integrating 2D SAXS data over 2θ.

of the detector plane and increases counter-clockwise. Regions of interest can be integrated over X or 2θ to produce intensity vs. 2θ or X data sets, respectively. The MD intercepts the detector at $X \cong 25°$ and at $205 \pm 5°$, i.e. along the line of scattering seen in Fig. 2. The intensity vs. X plots for the three films in Series I are shown in Fig. 3. It is obvious that all three films possess preferred lamellar orientations. Two strong peaks, 180° apart from each other, are observed for film A-1 (Fig. 3). The position of the peaks reveals that the long period in film A-1 lies along the MD, i.e. the crystalline lamellae are stacked preferentially along the MD. If examined closely, the intensity vs. X plot for film A-1 also shows two weak peaks, which are 90° from the two strong peaks, corresponding to the long period along the TD. Note that film A-1 was blown by the process with the lowest neck height. When the neck height is increased in Series I, as in the case of films A-2 and A-3, all four peaks are clearly visible (Fig. 3). The relative intensities of SAXS peaks indicate that for film A-2, which was blown using the intermediate neck height, the majority of lamellae are stacked along the MD. However, for the film made by the longest neck height, i.e. film A-3, the majority of lamellae are stacked along the TD. These observations suggest that films A-1, A-2 and A-3 have two preferred orientations of lamellae. One set of peaks corresponds to the lamellae stacked along the MD, while the other corresponds to the lamellae stacked along the TD.

TEM was performed in order to observe the arrangement of lamellae in the films directly. The TEM micrographs of the three films in Series I are shown in Figs. 4–6. As expected, a row-oriented crystalline structure is clearly observed with the lamellae stacked along the MD in all three films (Figs. 4a, 5a and 6a). Interestingly, when the TD–ND plane of these films is inspected using TEM, the row-oriented crystalline structure is also observed (Figs. 4b, 5b and 6b). The lamellae observed in this plane are stacked along the TD. The frequency by which the row-oriented structure can be found in the TD–ND plane varies from film to film. Film A-3 shows the highest frequency of this structure and film A-1 the lowest.

Based on the TEM and SAXS results, it is evident that an orthogonally-oriented, row-nucleated structure exists in the HDPE blown films. This structure consists of two superimposed row-oriented textures. In one texture, the lamellae are coherently stacked along the MD, i.e. the lamellar normal is oriented along the MD. In the other texture, the lamellar normal is oriented along the TD. This morphological feature is similar to that found by Dormier et al. [18].

The IR dichroic ratios and the calculated orientation functions are listed in Table 2. Note that the orientation functions determined here are uniaxial orientation functions. Although they are not sufficient to describe the biaxially-oriented crystalline textures in blown films, they can be used to quantify the overall orientation of the axes of the crystal unit cells with respect to a reference direction (the MD in this case). This overall crystallographic orientation is the result of the superimposition of the two row-oriented crystalline textures. For the three films in Series I, IR dichroism results show that the c-axis is preferentially oriented along the MD, and the a- and b-axes lie toward the TD–ND plane. The c-axis orientation along the MD increases in the order of A-3, A-2 and A-1. This result is consistent with both TEM and SAXS results.

In these HDPE films, the numbers of lamellae distributed in the two textures are not equal, but vary with processing conditions. There is an increasing tendency toward a single MD-stacked lamellar texture as the neck height decreases. For film A-1, which is blown under the lowest neck height condition, the crystalline texture is very close to a single MD-stacked texture. IR dichroism study shows that c-axis is preferentially oriented along the MD, and a- and b-axes lie toward the TD–ND plane in film A-1. This implies that the MD-stacked texture is a c-texture (Keller/Machin II morphology). For film A-3, although the majority of lamellae are oriented perpendicular to the TD, IR dichroism still shows a preferred c-axis orientation in the MD. This implies that either the orientation in MD-stacked texture is more

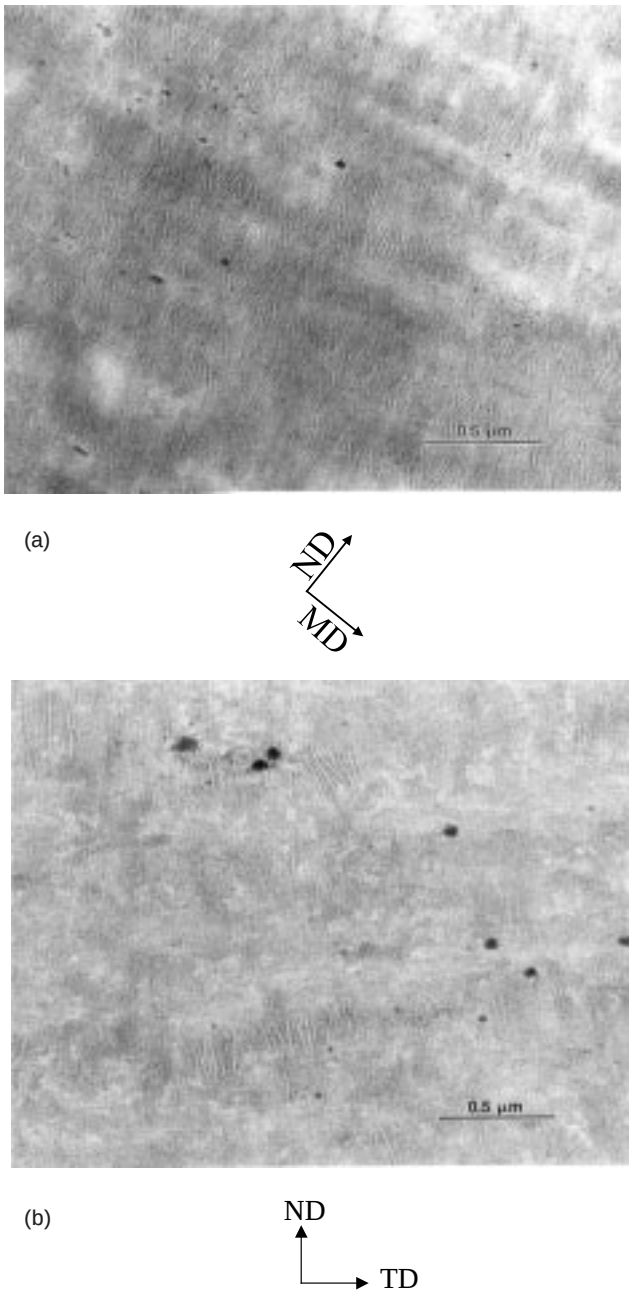

Fig. 4. TEM micrographs of film A-1 taken in: (a) MD–ND plane, and (b) TD–ND plane.

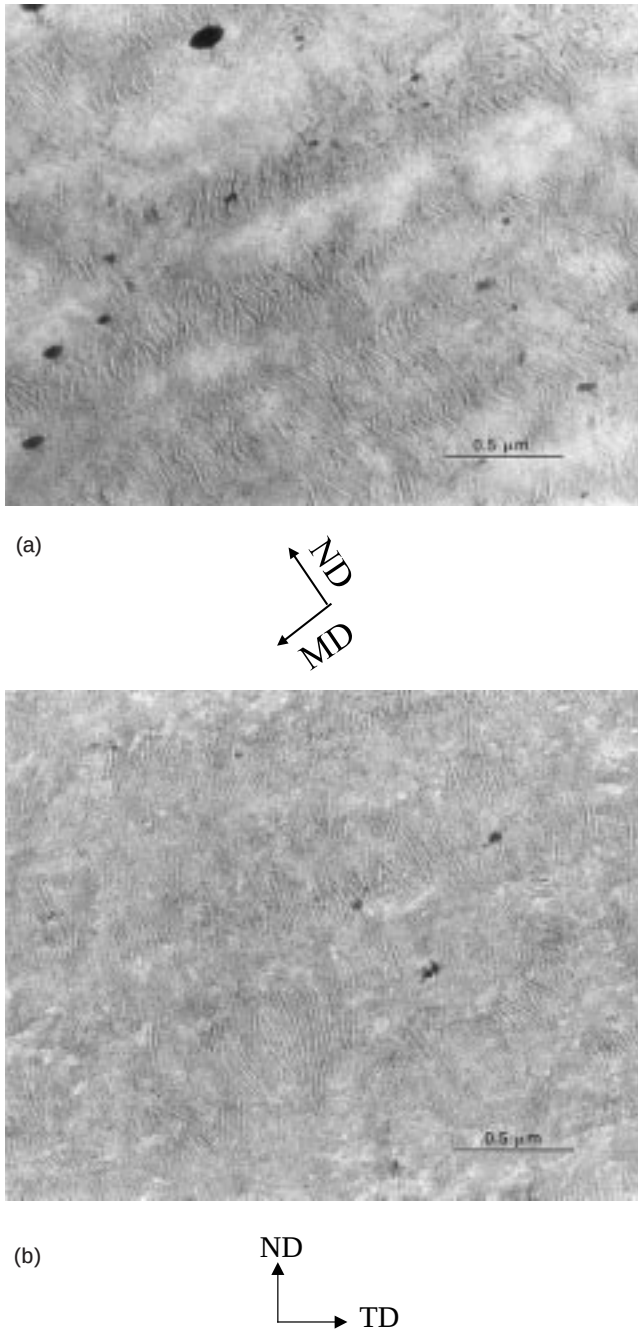

Fig. 5. TEM micrographs of film A-2 taken in: (a) MD–ND plane, and (b) TD–ND plane.

coherent, or the TD-stacked texture is not a *c*-texture in nature. At this stage, we cannot definitely determine the type (Keller/Machin I or II) of the TD-stacked texture in these HDPE films.

In Series II, films A-2, B-1 and C-1 were blown from different resins but using the same neck height and similar processing conditions. The SAXS patterns of films B-1 and C-1 are also shown in Fig. 3. The same transition can be observed from the dominance of the MD-stacked texture to the dominance of the TD-stacked texture as in Series I. TEM micrographs (Figs. 7 and 8) and IR dichroism data (Table 2) also support this trend. In film B-1, the MD-stacked texture dominates. In film A-2, the MD-stacked and TD-stacked textures are more balanced with the MD-stacked texture still dominant. Film C-1 has a dominant TD-stacked texture. This means that a particular film morphology can be achieved either by adjusting processing conditions or changing resin properties.

The superimposition of the two row-oriented crystalline

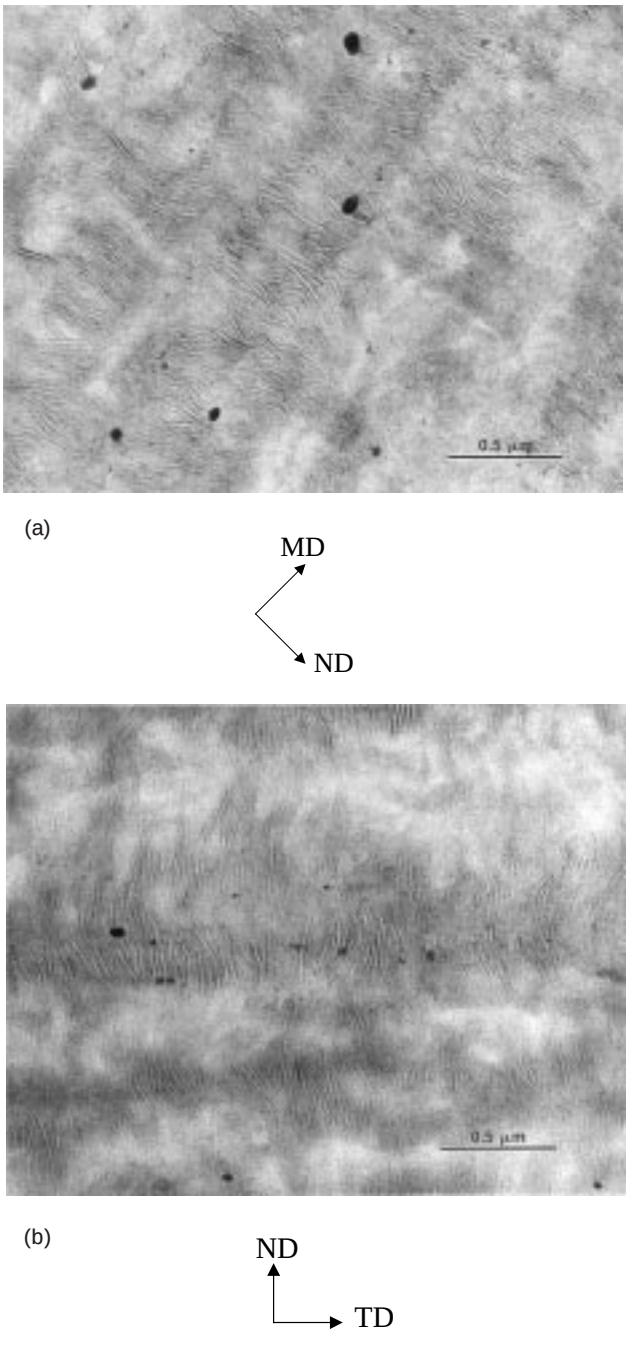

Fig. 6. TEM micrographs of film A-3 taken in: (a) MD–ND plane, and (b) TD–ND plane.

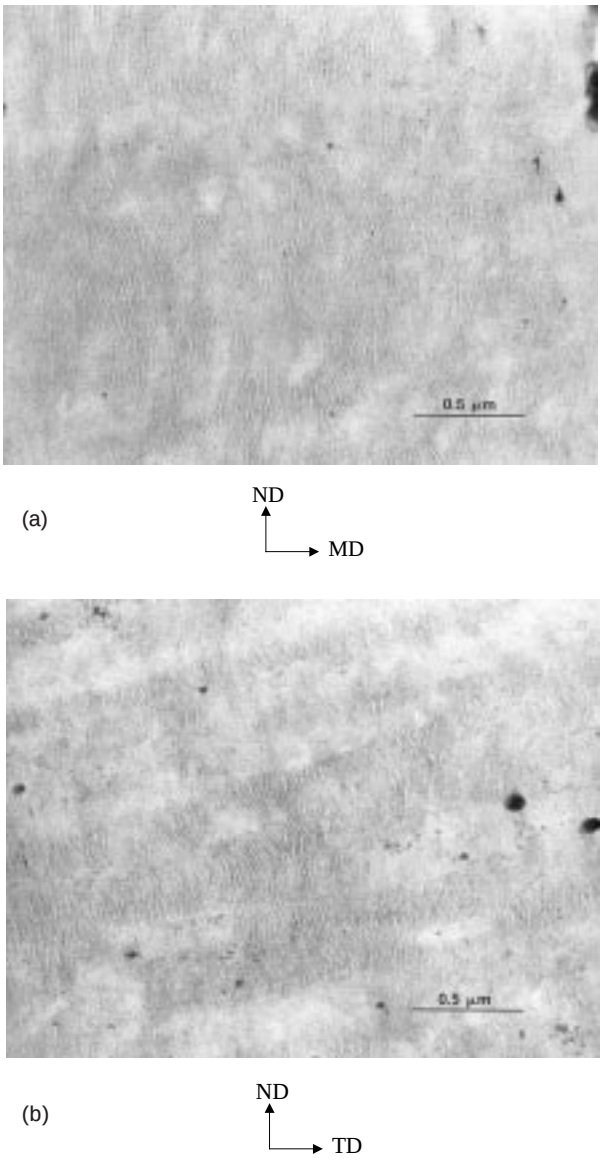

Fig. 7. TEM micrographs of film B-1 taken in: (a) MD–ND plane, and (b) TD–ND plane.

textures in the HDPE blown films suggests that two distinct crystallization processes exist during the blowing of the HDPE films. Before the bubble expansion region (Fig. 1), some polymer chains are sufficiently extended along the MD to nucleate stress-induced crystallization [18]. The resulting row-oriented lamellae are stacked along the MD. In the bubble expansion region, a significant number of polymer chains are still sufficiently mobile to allow TD stretching to nucleate another stage of stress crystallization, which gives the second row-oriented crystalline texture.

The region between the die face and the bubble expansion zone provides a region of low elongation rate in which a portion of the MD chain orientation introduced in the die can relax [23–26]. The higher the neck height, the longer the time available for the MD chain orientation introduced in the die to relax, and thus fewer extended chains remain for nucleating the crystallization that forms the MD-oriented lamellar stacks. Of course, once the melt exits from the die, the extensional strain imposed by the drawing in the MD causes additional MD chain orientation. Both the extension process and the relaxation process take place in the stalk region. Since the three films in Series I were blown

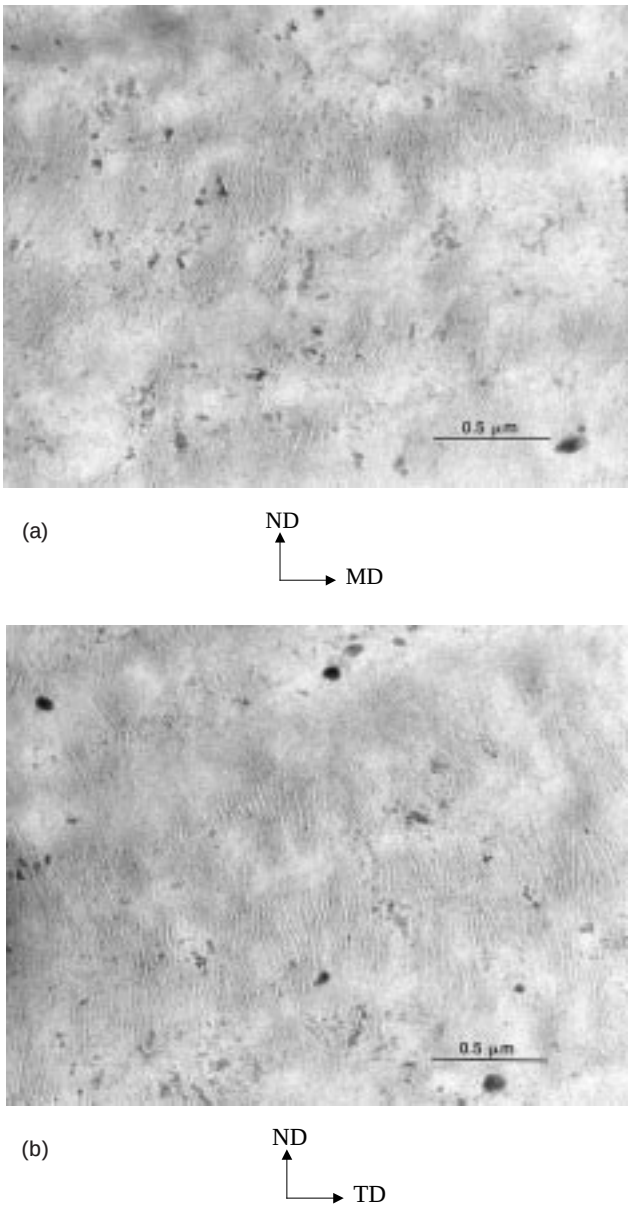

Fig. 8. TEM micrographs of film C-1 taken in: (a) MD–ND plane, and (b) TD–ND plane.

using the same draw ratio and line speed, the effect of the drawing in the MD is more or less equal for the three films. In this case, the neck height plays the major role in causing different morphologies in the resultant films. Moreover, in the film blowing process, the neck height is directly related to the cooling rate. As the neck height increases, the cooling rate of the polymer melt decreases. Consequently, for a lower neck height, a higher cooling rate and a larger number of nucleation sites lead to a larger portion of crystallization occurring in the stalk region. This gives rise to a dominant MD-stacked crystalline texture. When the neck height is increased, an increased portion of crystallization occurs in and beyond the bubble expansion region and a larger number of TD-stacked lamellae are formed. In the case where the neck height is sufficiently high, the TD-stacked crystalline texture can become dominant.

In Series II, the cause for the variation of crystalline texture is more complicated. The three films were blown from different resins. Different resins require somewhat different processing parameters for stable bubble formation. Thus, the processing conditions for the three films are not exactly same. Since the relaxation of polymer chain orientation during the film blowing process plays an important role in the structure formation of blown films, the resin melt relaxation time should have a significant influence on the crystalline texture of blown films. The melt relaxation time is dictated by melt temperature and the nature of resin [27–30], both of which vary in Series II. Therefore, it is difficult to unambiguously identify the cause(s) for the formation of the different morphologies found in Series II.

3.2. Structure–property relationship

Semicrystalline polymers can be considered to consist of crystalline lamellae held together by tie chains and separated by an amorphous phase. When stressed, what occurs first is the deformation at the crystalline lamella and amorphous layer level. Three deformation modes, namely lamellar separation, lamellar shear and lamellar rotation, can be postulated at this structural level [31]. Since the lamellae are held together by tie chains, these lamellar dislocations are restricted to small magnitudes before the disruption of the lamellae at the crystallographic level occurs. The deformation mechanisms at the crystallographic level involve chain slip and transverse slip, mechanical twinning, martenistic phase transformation, decrystallization and recrystallization processes [31–34].

If the crystalline lamellae in a film are uniaxially-oriented perpendicular to the MD, the film can be viewed as a ‘laminated composite’ of a hard crystalline phase and a soft amorphous phase stacked along the MD [19]. When stretched in the MD, the ‘composite’ can be considered as being deformed in an iso-stress pattern. Therefore, the modulus is dominated by that of the soft, amorphous phase. Furthermore, lamellar separation is the dominant deformation mechanism at first. The extent of separation is limited because of the existence of tie chains. Upon further stretching, the crystalline lamellae have to deform to allow higher straining. This results in the yielding of the film. On the other hand, when stretched in the TD, the composite can be considered as being deformed in an iso-strain pattern; therefore, the modulus is dominated by that of the hard, crystalline phase. When the film is stretched along the TD, deformation at the level of the crystalline lamella and amorphous layer, i.e. lamellar separation, lamellar shear and lamellar rotation, is largely restricted. Consequently, the film yields at a small magnitude of strain. In the MD stretching, chain slip is the dominant deformation mode of the crystalline phase following yielding. Conversely, the

Table 2
Dichroic ratios, orientation functions and crystallinities of the HDPE blown films studied

Samples	A-1	A-2	A-3	B-1	C-1
D_{730}	0.873	0.883	0.918	0.738	0.906
D_{720}	0.627	0.795	0.886	0.475	1.132
f_a	−0.0438	−0.0407	−0.0282	−0.0956	−0.0325
f_b	−0.1536	−0.0732	−0.0396	−0.2120	0.0420
f_c	0.1974	0.1139	0.0678	0.3076	−0.0096
Crystallinity[a] (%)	57.5	55.5	58.6	61.4	55.5

[a] Measured by the film manufacturers using density column.

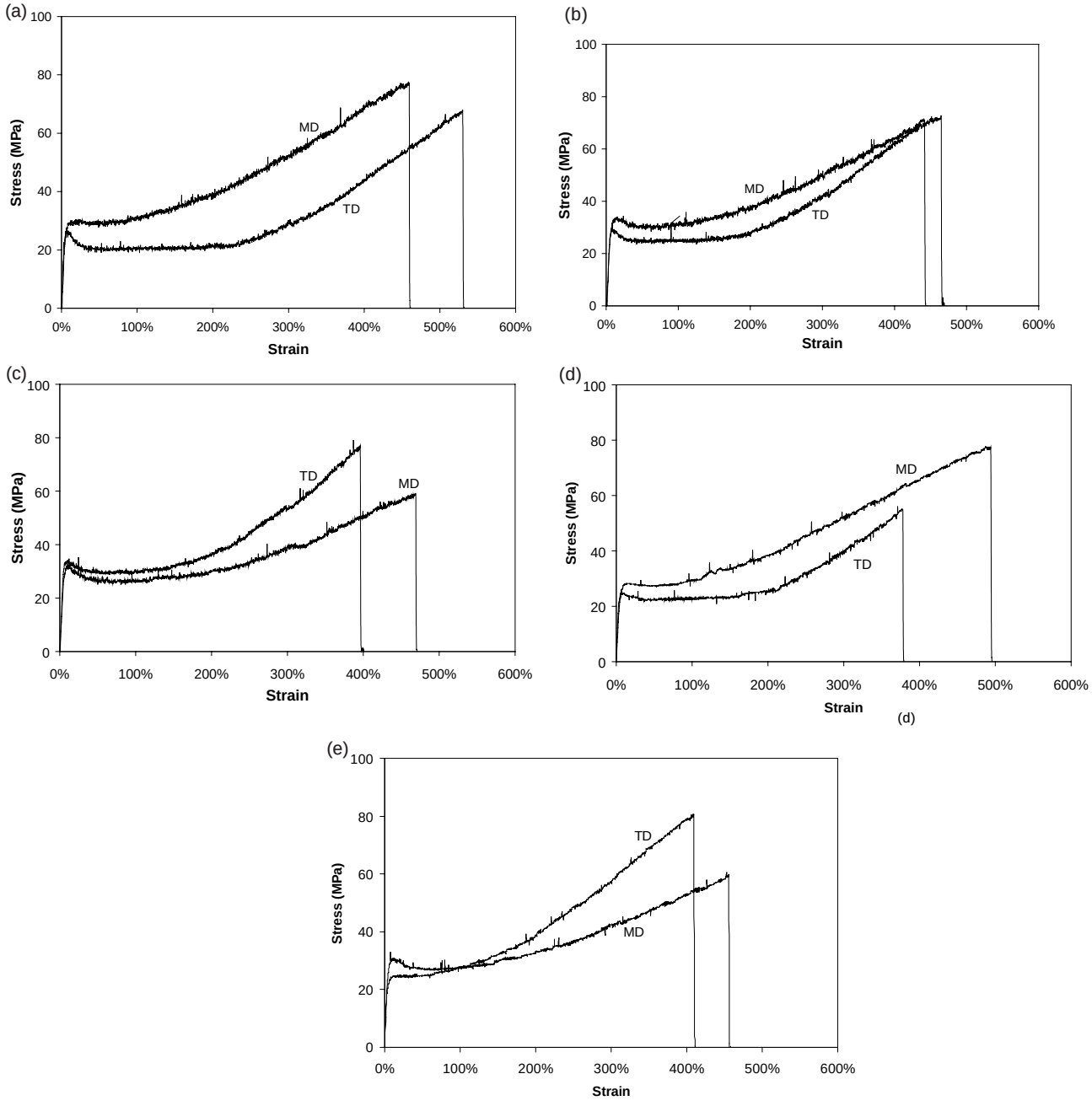

Fig. 9. Engineering stress–strain curves of: (a) film A-1, (b) film A-2, (c) film A-3, (d) film B-1, and (e) film C-1.

Table 3
Mechanical properties of the HDPE blown films studied

Samples	A-1	A-2	A-3	B-1	C-1
MD Young's modulus (MPa)	830 ± 50	830 ± 80	920 ± 50	770 ± 50	870 ± 50
TD Young's modulus (MPa)	1020 ± 40	850 ± 40	860 ± 70	890 ± 70	730 ± 20
MD Elmendorf tear[a] (g)	11.0	16.6	23.1	14.0	24.0
TD Elmendorf tear[a] (g)	36.4	19.9	13.6	42.3	14.1
Dart impact resistance[a] (g)	330	290	220	400	240

[a] Provided by the film manufacturers.

break-up of the crystalline lamellae, the pull-out of the chains from the lamellae and the transverse slip are the major deformation mechanisms of the crystallites in the TD stretching. The pull-out of polymer chains in this case is perpendicular to the lamellar normal. It is clear that the pull-out of chains in this direction is much easier than the chain slip, and is basically a cold-drawing process.

The engineering stress–strain curves of the five HDPE films are shown in Fig. 9. In Series I, the TD stress–strain curve for film A-1 shows a yield peak and a horizontal plateau before strain hardening (Fig. 9a). This is due to the fact that the MD-stacked texture is the dominant texture, and the overall morphology is close to a unimodal orientation. In the MD tensile test of film A-1, strain hardening occurs soon after yielding, and the stress level of the MD stress–strain curve is higher than that of the TD stress–strain curve. For film A-2, the stress–strain curves for the MD and TD stretches get closer (Fig. 9b). This can be correlated to increased bimodal crystalline orientation feature in this film. Since the MD-stacked texture is still dominant in film A-2, the stress level of the MD stress–strain curve is higher than that of the TD stress–strain curve. The TD-stacked texture becomes dominant in film A-3. As a result, the stress level of the TD stress–strain curve exceeds that of the MD stress–strain curve (Fig. 9c). In Series II, a trend in tensile behavior similar to that in Series I can be observed. Films A-1 and B-1 have similar tensile behaviors because of the structural similarity between them. For the same reason, films A-3 and C-1 have similar tensile behaviors.

The mechanical properties of the five HDPE blown films are listed in Table 3. As illustrated by the laminated composite model, the trend in tensile modulus for the HDPE films can be easily correlated to their crystal orientation features. For films A-1 and B-1, the TD tensile modulus is higher than the MD tensile modulus, because the majority of the lamellae are stacked perpendicular to the MD. With its lamellae more biaxially-oriented, film A-2 possesses similar moduli in the MD and TD. Films A-3 and C-1 have higher moduli in the MD, because more lamellae are stacked along the TD in these films.

The trend in tear strength can also be correlated to the feature of dual crystalline texture. In films A-1 and B-1, the MD-stacked crystalline texture is dominant, giving a much higher Elmendorf tear strength in the TD than in the MD. Conversely, in films A-3 and C-1 the TD-stacked crystalline texture is dominant. As a result, the MD Elmendorf tear strength is much higher than the TD tear strength. In film A-2, the MD- and TD-stacked crystalline texture are more balanced. This results in more balanced tear strengths in the MD and TD.

The dart drop impact resistance of blown films is commonly considered to be related to the anisotropic characteristics of both their structure and mechanical properties

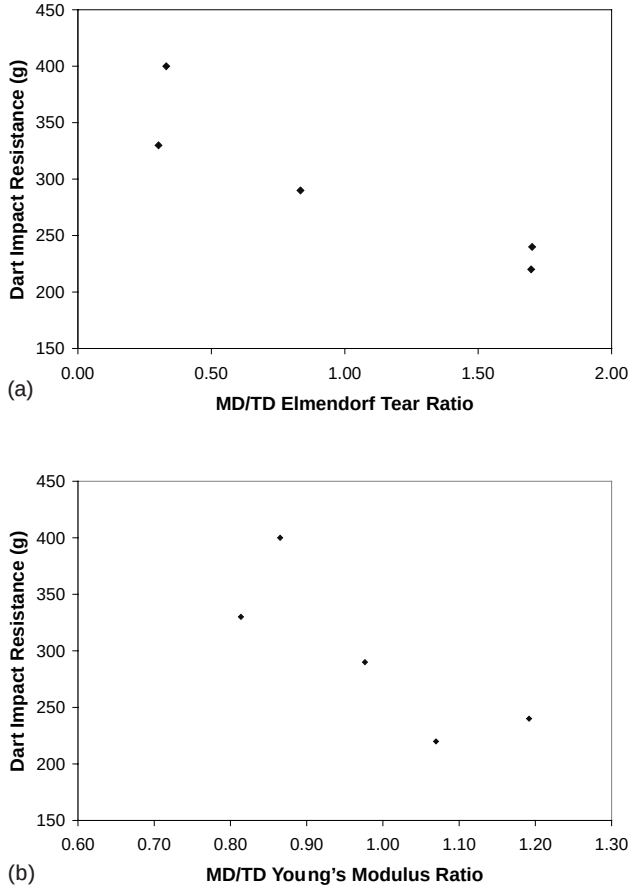

Fig. 10. Dart drop impact resistance plotted as a function of: (a) Elmendorf tear strength, and (b) Young's modulus.

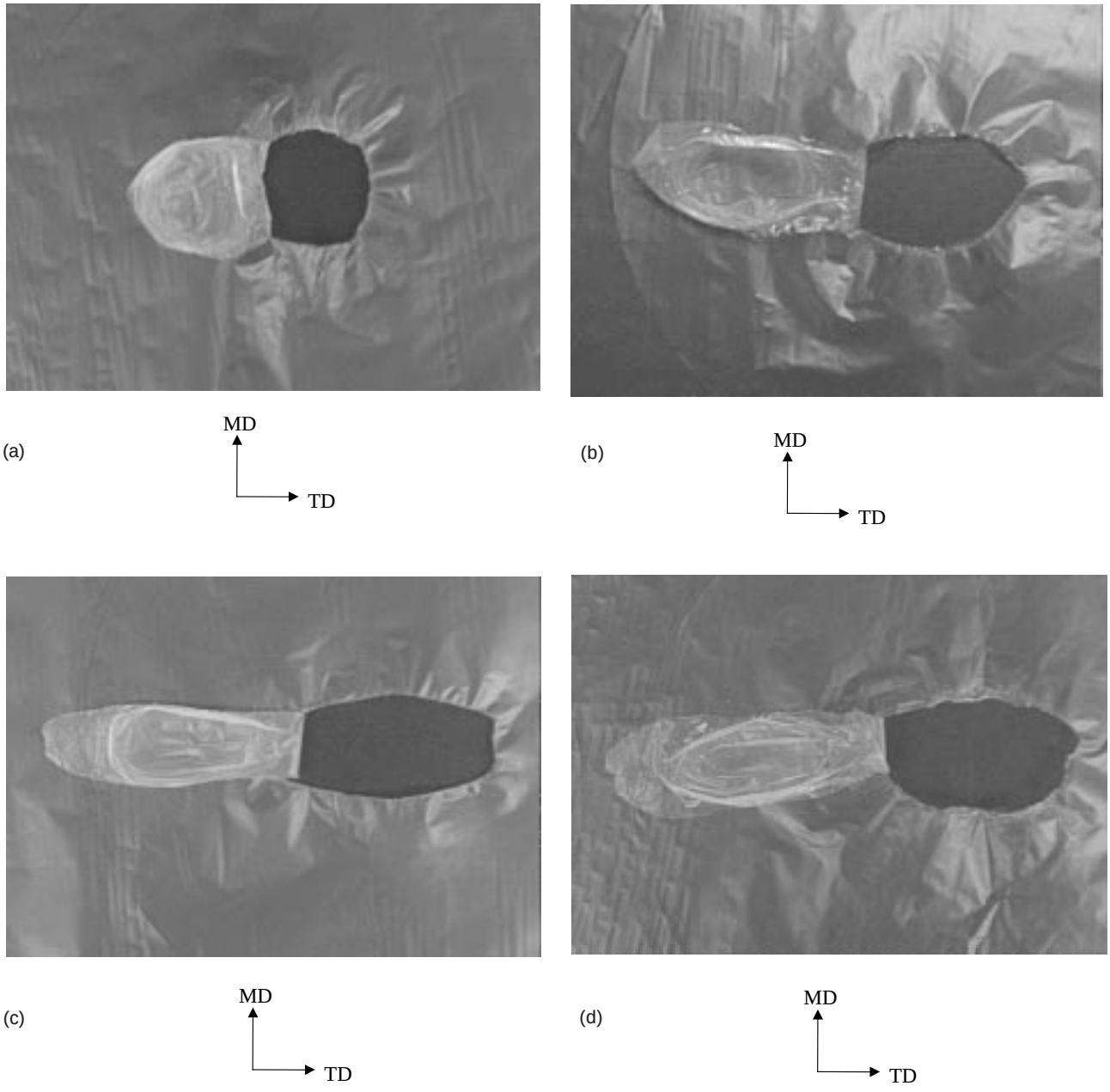

Fig. 11. Photographs of the failed specimens in dart drop impact test of: (a) film A-1, (b) film A-2, (c) film A-3, (d) film B-1, and (e) film C-1.

[35]. A good balance in structure and mechanical properties between the MD and TD usually give a high dart drop impact strength. However, this is not true for the films in this study. The dart drop impact strength is plotted as a function of the MD/TD Elmendorf tear strength ratio (Fig. 10a) and the tensile modulus ratio (Fig. 10b) for the five films. Good tear and modulus balances do not give a high dart drop impact resistance. The dart drop impact strength increases with increasing TD Elmendorf tear strength for these films (Table 3). In terms of morphology, films A-1 and B-1 are the least balanced, but they have the highest dart drop impact strength. Films A-2, A-3 and C-1 are more balanced structurally, but their dart drop impact strengths are lower. It appears that the larger the MD-stacked crystalline component, the higher the dart drop impact resistance.

As discussed in the previous section, the formation of the MD-stacked crystalline texture starts earlier than that of the TD-stacked crystalline texture. At an earlier stage, the melt temperature is higher, thus the mobility of polymer chains is higher and a polymer chain has a better chance to fold into the same lamella. It can be speculated that the tie chain density in the TD-stacked texture is higher than that in the MD-stacked texture. Consequently, the TD-stacked texture

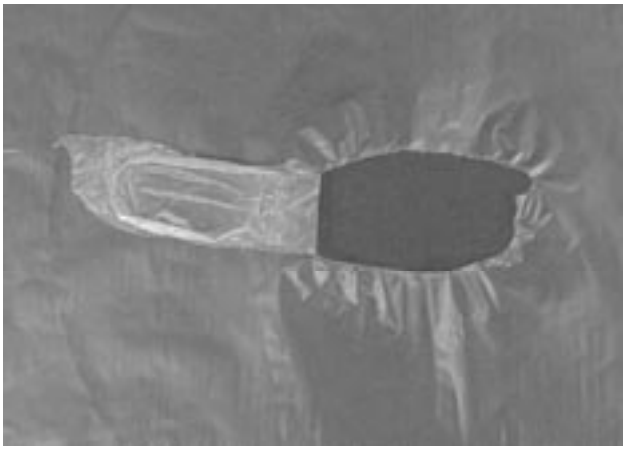

(e)

Fig. 11. (*continued*)

can withstand more load than the MD-stacked texture. The dart drop impact is basically a biaxial stretching process. If there are an equal number of MD- and TD-oriented lamellar stacks, the MD will be the weak direction for dart impact. To verify this, the failed dart impact test specimens were examined. It was observed that most specimens failed in the MD (the cracks propagate along the TD), except for film A-1 (Fig. 11). For film A-1, the specimens seemed to have failed simultaneously in the MD and TD. Note that film A-1 is a highly structurally unbalanced film, and many more lamellae are stacked along the MD than along the TD in this film. Therefore, the MD-oriented lamellar stacks are indeed relatively weak in dart impact compared to the TD-oriented lamellar stacks. A larger number of MD-oriented stacks are needed to gain the same strength as a small number of TD-oriented stacks. Therefore, in these HDPE films, the number of the MD-oriented stacks is more important for the dart drop impact resistance.

The orthogonally-oriented, dual crystalline texture is an important morphological feature in HDPE blown films. The assessment of this structure can greatly help interpret the orientation-dependent mechanical properties of the films. There is still a need to analyze each individual component texture in detail. The characteristics of the orientation in each texture, as well as the type of the TD-stacked texture, should be addressed. Further investigation of this aspect is still underway.

4. Conclusion

The morphological features of selected HDPE blown films have been carefully studied. In these films, an orthogonally-oriented, dual crystalline texture is found. This structure consists of two superimposed row-oriented crystalline textures, i.e. an MD-stacked texture and a TD-stacked texture. The lamellar populations in the two structures are affected greatly by the neck height of the film blowing process. The MD-stacked crystalline texture is found to be a *c*-texture. The trends in the mechanical properties of the HDPE films can be interpreted well in terms of the feature of the dual crystalline texture. The dart impact resistance appears to depend more on the MD-stacked row crystalline structure.

Acknowledgements

The authors would like to thank the Polyolefins Films Consortium (Equistar Chemical Company, Exxon-Mobil Chemical Company, Phillips Petroleum Company and Eastman Chemical Company) at Texas A & M University for financial support and providing the PE blown films. Financial support from NSF (Grant # NSF/CTS-9705467) is also appreciated. Special thanks are due to E.I. Garcia-Meitin and Helga Sittertz-Bhatkar for their valuable instruction for the TEM work. T.P.R. acknowledges the financial support from Sandia National Laboratories operated for the US Department of Energy under contract number DEAC04-99AL85000.

References

[1] Holmes DR, Palmer RP. J Polym Sci 1958;31:345.
[2] Aggarwal SL, Tilley GP, Sweeting OJ. J Appl Polym Sci 1959;1:91.
[3] Keller A. Nature 1954;174:826.
[4] Keller A. J Polym Sci 1955;15:31.
[5] Lindenmeyer PH, Lustig SJ. J Appl Polym Sci 1965;9:227.
[6] Keller A, Machin MJ. J Macromol Sci 1967;B1:41.
[7] Desper CD. J Appl Polym Sci 1969;13:169.
[8] Kobayashi K, Nagasawa T. J Polym Sci: Part C 1966;15:163.
[9] Haudin JM. Ann Chim Fr 1980;5:513.
[10] Ashizawa H, Spruiell JE, White JL. Polym Engng Sci 1984;24:1035.
[11] Walenta E, Janke A, Hofmann D, Fanter D, Geiss D. Acta Polym 1986;37:557.
[12] Maddams W, Preedy J. J Appl Polym Sci 1978;22:2721.
[13] Maddams W, Preedy J. J Appl Polym Sci 1978;22:2739.
[14] Maddams W, Preedy J. J Appl Polym Sci 1978;22:2751.
[15] Yu TH, Wilkes GL. Polymer 1996;37:4675.
[16] Choi K, Spruiell JE, White JL. J Polym Sci, Polym Phys Ed 1982;20:27.
[17] Kwack TH, Han CD, Vickers ME. J Appl Polym Sci 1988;35:363.
[18] Dormier EJ et al. Proceedings of the 47th Society of Plastics Engineers Annual Technical Conference (ANTEC), New York, May, 1989. p. 696.
[19] Zhou H, Wilkes GL. J Mater Sci 1998;33:287.
[20] Kissin YV. J Polym Sci, Polym Phys Ed 1992;30:1165.
[21] Read BE, Stein RS. Macromolecules 1968;1(2):116.
[22] Rieker TP, Hubbard PF. Rev Sci Inst 1998;69:3504.
[23] Winter HH. Pure Appl Chem 1984;55:943.
[24] Kanai T, Kimura M, Asano Y. J Plast Film Sheeting 1986;2:224.
[25] Shirodkar PP, Schregenberger SD. Proceedings of the 45th Society of Plastics Engineers Annual Technical Conference (ANTEC), Los Angeles, May, 1987. p. 37.
[26] Lu J, Sue HJ, Rieker TP. J Mater Sci 2000;35:5169.
[27] Graessley WW. Adv Polym Sci 1974;16:70.

[28] Graessley WW. Adv Polym Sci 1974;16:132.
[29] Wilkes GL. J Chem Educ 1981;58:880.
[30] Yu TH, Wilkes GL. J Rheol 1996;40:1079.
[31] Bowden PB, Young RJ. J Mater Sci 1974;9:2034.
[32] Lin L, Argon AS. J Mater Sci 1994;29:294.
[33] Shinozaki DM, Groves GW. J Mater Sci 1973;8:1021.
[34] Hay IL, Keller A. J Polym Sci 1970;30:289.
[35] Kim Y, et al. J Appl Polym Sci 1997;63:289.